Separation Science and Technology
Publication details, including instructions for authors and subscription information:
http://www.informaworld.com/smpp/title~content=t713708471

Determination of Mass Transfer Rates in PVDF and PTFE Hollow Fiber Membranes for CO_2 Absorption

Sun-Hwa Yeon[a]; Bongkuk Sea[a]; You-In Park[a]; Kew-Ho Lee[a]
[a] Membranes and Separation Research Center, Korea Research Institute of Chemical Technology, Taejon, "KR" South Korea

Online publication date: 20 February 2003

To cite this Article Yeon, Sun-Hwa , Sea, Bongkuk , Park, You-In and Lee, Kew-Ho(2003) 'Determination of Mass Transfer Rates in PVDF and PTFE Hollow Fiber Membranes for CO_2 Absorption', Separation Science and Technology, 38: 2, 271 — 293
To link to this Article: DOI: 10.1081/SS-120016575
URL: http://dx.doi.org/10.1081/SS-120016575

MARCEL DEKKER, INC. • 270 MADISON AVENUE • NEW YORK, NY 10016

SEPARATION SCIENCE AND TECHNOLOGY
Vol. 38, No. 2, pp. 271–293, 2003

Determination of Mass Transfer Rates in PVDF and PTFE Hollow Fiber Membranes for CO_2 Absorption

Sun-Hwa Yeon, Bongkuk Sea, You-In Park, and Kew-Ho Lee*

Membranes and Separation Research Center, Korea Research Institute of Chemical Technology, Taejon, South Korea

ABSTRACT

The gas–liquid mass transfer accompanied by chemical reaction was studied in a membrane absorber for the separation of CO_2 from mixture gases. The membranes used were made of polytetrafluoroethylene (PTFE) and polyvinylidenefluoride (PVDF) and the aqueous MEA solution was used as an absorbent possessing a high chemical reaction with carbon dioxide. The numerical model for the CO_2 concentration profile in a fiber was developed, and the influence of its flux on the external mass transfer resistances, including gas and membrane, was simulated with this numerical model and compared with the experimental results. Experimentally, it is found that absorption rate per surface area was higher in PVDF membrane than that in PTFE membrane because of the non-wetted condition of membrane pore. The membrane pore wetted with an absorbent showed the low absorption performance by high membrane resistance. We could predict the liquid resistance and

*Correspondence: Kew-Ho Lee, Membranes and Separation Research Center, Korea Research Institute of Chemical Technology, Taejon, 305-600, Korea; Fax: +82-42-861-4151; E-mail: khlee@pado.krict.re.kr.

DOI: 10.1081/SS-120016575 0149-6395 (Print); 1520-5754 (Online)

membrane–gas resistance (external resistance) from experimental and numerical mass transfer coefficient data.

Key Words: Carbon dioxide; Gas absorption; Hollow fiber; Membrane contactor; Numerical modeling; Mass transfer coefficient.

INTRODUCTION

Recently many countries agreed to reduce emissions of greenhouse gases into the atmosphere or at least to keep them at the current level at the Kyoto Conference. Carbon dioxide has been proven to be 80% of greenhouse gases, contributing to the increase of the earth's surface temperature. It is reported that half of the CO_2 emissions are produced by industry and power plants using fossil fuels.[1]

The gas absorption process for removing the carbon dioxide can be carried out in many reactors, such as bubble columns, packed towers, venturi scrubber, and sieve trays. A new type of gas absorber[2,3] is the microporous hollow fiber membrane module, which has the advantages of a large interfacial area, independent gas–liquid phase control, no flooding and no channeling, and others. The amount of interfacial area in the hollow fiber modules is about $10000\,m^2/m^3$, while $1000\,m^2/m^3$ is reported in that of the conventional absorbers.[4] These advantages of the hollow fiber membrane contactor have been proved through many studies. Karoor and Sirkar[5] studied the absorption of CO_2 and SO_2 from CO_2/N_2 and SO_2/air mixtures, respectively, into water using a paralled flow module employing microporous polypropylene fibers. Kreulen et al.[6] studied the absorption of CO_2 into water/glycerol using polypropylene or polysulfone hollow fibers. Falk-Pedersen and Daninstrom[7] studied the separation of CO_2 from offshore gas turbine exhaust using membrane gas/liquid contactors in both the absorber and the desorber and optimized the process with respect to sizes, weight, and cost. There is also much research on CO_2 absorption behavior using various kind of hollow fibers and absorbents. They show that the advantage of the increased contact area is greater than the disadvantage of the membrane resistance.[8–14]

In addition, many studies on the characterization of the mass transfer behavior for gas absorption into various absorbents have been conducted.[15–19] Qi and Cussler[15–17] developed a theory for the operation of hollow fiber membrane modules, and investigated mass transfer coefficients in the liquid phase. They also studied overall mass transfer coefficients, including resistances in both liquid and membrane, and compared

the performance of hollow fibers with that of packed towers. Sirkar et al.[18] conducted an experimental study of gas–liquid contacting and reported the mass-transfer performance characteristics of hollow fiber devices that employ transverse liquid flow over microporous hydrophobic fibers present in a mat wrapped around a central feeder tube. Kreulen[20] also studied the hollow fiber membrane as gas–liquid contactors in the case of physical and chemical mass transfer process both theoretically and experimentally.

The mass transfer rate in the membrane contactor module is limited by the mass transfer resistance in the gas, liquid phase, and additional resistance introduced by the membrane itself. Although the interfacial area of the membrane is much more than conventional absorbers, the increase of its additional resistance can cause a decrease in the mass transfer capacity of the membrane due to the resistance of the membrane itself, a resistance that is increased if the liquid wets the membrane. To minimize the membrane resistance, pores of hollow fiber should be controlled under the non-wetted (gas-filled) condition. In this condition, the advantages of the membrane contactor for gas absorption can be maximized.

In the present study, the gas absorption accompanied by the chemical reaction using hollow fiber membrane absorbers was investigated in the theoretical and experimental aspects. A numerical model for mass transfer in gas absorption was developed and the CO_2 absorption rate was simulated according to gas, liquid velocity, and external mass transfer coefficient, including mass transfer in the gas phase and membrane. Using PTFE and PVDF membrane modules, CO_2 removal efficiency and flux with liquid and gas velocity were experimentally investigated. Overall mass transfer coefficients were calculated. Through the comparison between the experimental results and the numerical model, we predicted the external and liquid resistances in CO_2 absorption by the PTFE and PVDF hollow fiber membranes.

THEORY

Film Model

The mass transfer between gas and liquid though the hollow fiber membrane contactor occurs in three parts; gas film, membrane, and liquid film[2] as shown in Fig. 1. The CO_2 flux per unit fiber length at any

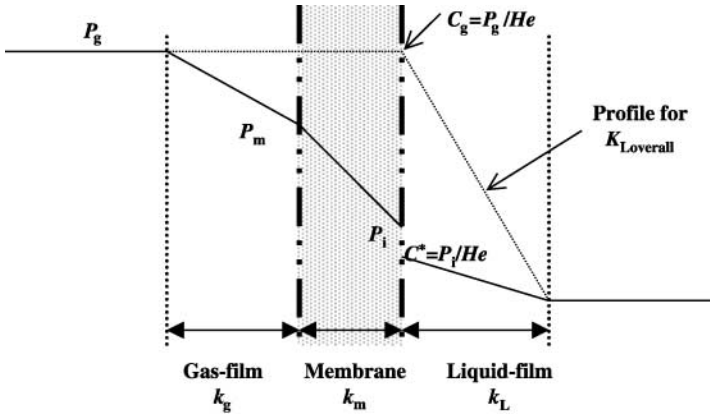

Figure 1. Film model for mass transfer across an ideal non-wetted membrane.[2]

cross-section, N can be expressed by Eq. (1).

$$N(n\pi d_i) = K_L(n\pi d_i)(P_g/He) = Ek_L(n\pi d_i)(P_i/He)$$
$$= (k_m/RT)(n\pi d_0)(P_m - P_i) = k_g(n\pi d_0)(P_g - P_m) \quad (1)$$

where k_L, k_m, and k_g indicate the mass transfer coefficients (m/s) of the liquid phase, membrane, and gas phase, respectively; n is the number of the fiber; d_i and d_o are inside and outside diameter of the fiber: P_g, P_i, and P_m, are CO_2 partial pressures in the bulk gas phase, membrane–liquid interface, and gas–membrane interface, respectively (kPa); He is the Henry's constant (m^3 kPa/mol); and E is enhancement factor (−). The overall resistance in gas–liquid mass transfer through the porous hollow fiber membrane contactor can be expressed as the following Eq. (2).

$$(1/K_L) = (1/Ek_L) + (1/k_m)(RT/He)(d_i/d_o) + (1/k_g)(1/He)(d_i/d_o) \quad (2)$$

If we define the sum of membrane and gas phase resistance as external resistance, $1/k_{ex}$, such as Eq. (2a), the overall resistance in the liquid phase is summarized by Eq. (2b)

$$(1/k_{ex}) = (1/k_m)(RT/He)(d_i/d_o) + (1/k_g)(1/He)(d_i/d_o) \quad (2a)$$

$$1/K_L = (1/Ek_L) + (1/k_{ex}) \quad (2b)$$

If we assume that the flow on both the shell and tube side depends on the ideal plug-flow behavior, the average driving force on the gas side is the log-mean

partial pressure of the solute (CO_2). The overall mass transfer coefficient, K_L can be obtained by Eq. (3).

$$K_L a = R/(\Delta P_{Lm}/He) \tag{3}$$

where R is CO_2 absorption rate(mol/m^3 s) per unit volume of the contactor; ΔP_{Lm} is the log-mean partial pressure of CO_2 calculated from Y_{Lm}, the log-mean of the inlet and outlet CO_2 concentration in the gas phase, and, the average column shell side pressure.

Mass Transfer in Chemical Reaction of Liquid Phase

In the hollow fibers used in this study, the liquid absorbent flows laminarily through the lumen side and the gas phase flows on the shell side in the module. It is assumed that in the liquid phase, an irreversible reaction of CO_2 takes place with the MEA, which is already present in the liquid. The concentration profile of each component in the liquid can be calculated from the differential mass balance that describes diffusion and forced convection in a medium that flows laminarily through a circular pipe. We can neglect the effect by the axial diffusion in a cylindrical coordinate system (Fig. 2) because the concentration gradient in the axial direction will be much smaller than that of the radial direction.[20] First, the radial velocity profile, v_r, which is formed

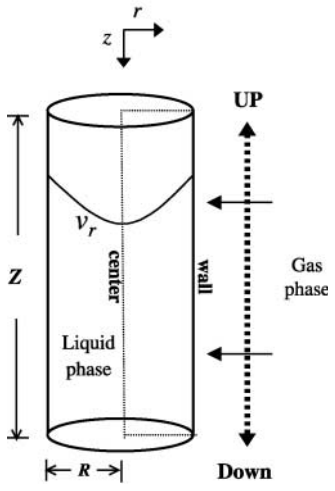

Figure 2. Cylindrical coordinate system in a membrane.

by forced convection under assuming a fully developed laminar flow in tube, is described by Eq. (4)

$$v_r = 2\bar{v}\left[1 - \left(\frac{r}{R}\right)^2\right] \tag{4}$$

Next, we can obtain Eqs. (5) and (6) by establishing the differential mass balance of CO_2 and MEA in the condition of a chemical reaction. Conveniently, the CO_2 and MEA are denoted as component A and B, respectively.

Component A (CO_2):

$$v_r \frac{\partial C_A}{\partial z} = D_A\left[\frac{1}{r}\frac{\partial}{\partial r}\left(r\frac{\partial C_A}{\partial r}\right)\right] - k_1 C_A C_B \tag{5}$$

Component B (MEA):

$$v_r \frac{\partial C_B}{\partial z} = D_B\left[\frac{1}{r}\frac{\partial}{\partial r}\left(r\frac{\partial C_B}{\partial r}\right)\right] - v_B k_1 C_A C_B \tag{6}$$

The following boundary conditions for three regions are imposed on the membrane system. At the membrane–liquid interface the flux of component A in the liquid phase is equal to the flux in the gas phase in which the external resistance included both the membrane and gas phase resistance because of the condition of non-wetted membrane.

$$D_A\left(\frac{\partial C_A}{\partial r}\right) = k_{ex}(C_{A,g} - C_{A,g,i}) \tag{7a}$$

where

$$k_{ex} = \frac{1}{\frac{1}{k_g} + \frac{1}{k_m}} \tag{7b}$$

Moreover, component B is nonvolatile:

$$\left(\frac{\partial C_B}{\partial r}\right)_{r=R} = 0 \tag{7c}$$

At the centerline of the tube, component A and B form a symmetric structure in that system.

$$\left(\frac{\partial C_A}{\partial z}\right)_{r=0} = 0 \tag{7d}$$

$$\left(\frac{\partial C_B}{\partial z}\right)_{r=0} = 0 \tag{7e}$$

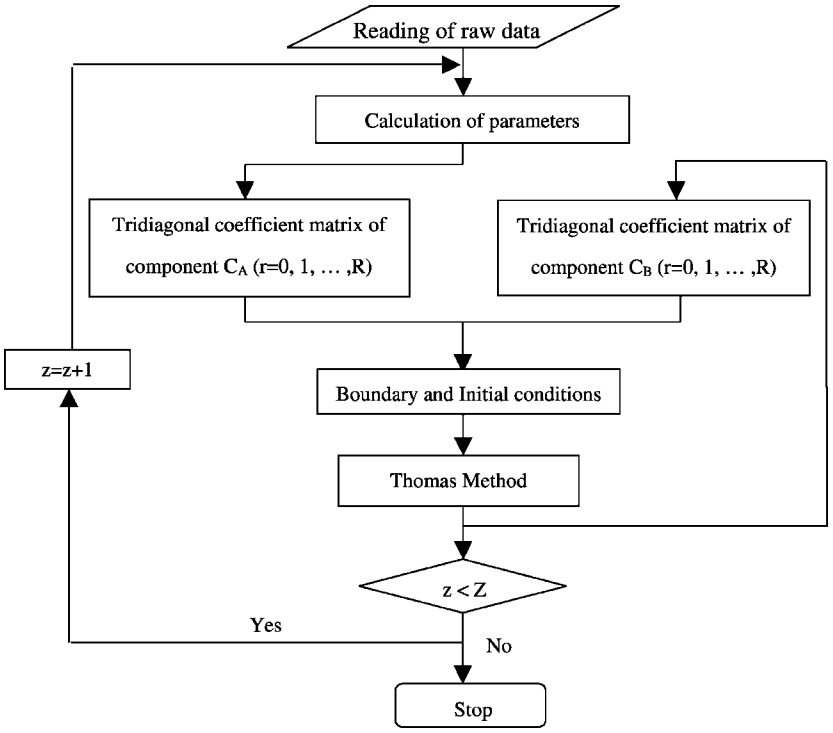

Figure 3. Alkgorithm for Crank–Nicholson method.

Initial conditions at z = 0 are:

$$C_A = 0 \quad \text{and} \quad C_B = C_{B0} \tag{7f}$$

The concentration profiles of component A and B are obtained numerically by using the Crank–Nicholson method, which is a good mathematical technique for solving the partial differential equation under the condition of several boundary regions. The algorithm for the simulation is shown is Fig. 3.

NUMERICAL RESULTS

To predict the concentration profiles of the CO_2 and MEA, a standard case, of which the variables are given in Table 1, was used. The data on this table are based on the experimental conditions of the following

Table 1. Conditions for calculation of calculation of concentration profile.

C_{Ag}	$10\,mol/m^3$
C_{BO}	$809\,mol/m^3$
D_A	$2 \times 10^{-9}\,m^2/sec$
D_B	$4 \times 10^{-9}\,m^2/sec$
k_1	$1 \times 10^{-3}\,m^3/(mol\,sec)$
M	0.49
v_B	2
R	$8.3 \times 10^{-4}m$
v_L	$4.43 \times 10^{-3}\,m/sec$
Z	$0.23\,m$

section. D_A is the diffusivity of CO_2 in MEA aqueous solution, D_B is the diffusivity of the amine in aqueous amine solution, and k_1 is reaction rate constant of CO_2 and MEA solution. These data were cited from the literature.[23–27] In the calculations, it is assumed that the bulk gas phase concentration is constant over the fiber length. The calculated concentration profile of CO_2 absorbed in liquid is presented in Fig. 4. In the direction of the diameter of one fiber, this figure shows the largest concentration gradient at the wall side of the fiber. This means that the gas–liquid mass transfer at the membrane interface is conducted mostly at the wall side of the fiber in which the numerous pores exists. In the direction of the fiber length, the absorbed CO_2 concentration is steeply increased at the up side of fiber and then slightly increased along the down side direction in the fiber's wall. This initial sudden behavior results from the active mass transfer between the fresh liquid and gas phase coming into the fiber's entrance. For a more detailed observation, Fig. 5 indicates the concentration profiles of CO_2 and MEA according to the fiber length direction for the different total fiber lengths. As explained in Fig. 4, the concentration of CO_2 is increased with the fiber's length while that of MEA is decreased due to chemical reaction of the two components. It means that the CO_2 flux decreases along the fiber length because the driving force is reduced toward the fiber's downside. We can expect from Fig. 6 that the increase of the initial concentration of the gas phase caused the increase of the total flux due to a high driving force, on the condition of constant external resistance. All the calculated fluxes for the different initial concentrations of component A showed a decrease with the fiber length. This appearance was brought about by the large consumption of the component MEA reacting with CO_2 at the fiber

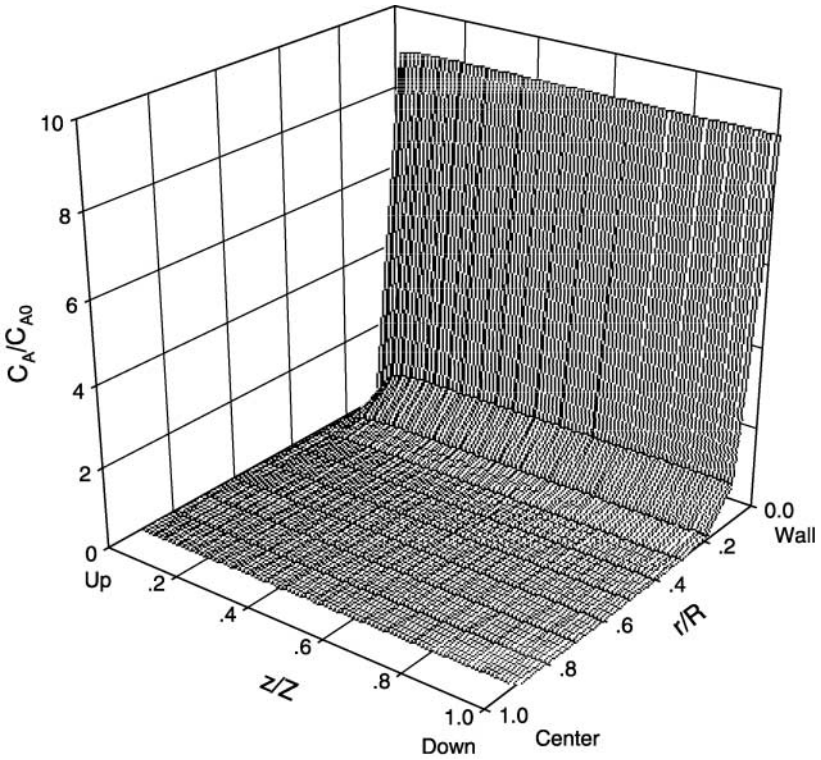

Figure 4. Absorbed CO_2 concentration profile in a hollow fiber. $k_{ex} = 0.001\,m/s$, Refer to Table 1 for the calculation parameters.

downside. Figure 7 presents the calculated fluxes of component A with the fiber length for the different initial concentrations of component B. As the C_{B0} was higher, the larger CO_2 flux appeared.

Figures 8 and 9 are the results to find out how the liquid velocity and external resistance affect the CO_2 flux in PVDF and PTFE membranes, respectively. The properties of these fibers are shown in Table 2 in which the data are used to calculate the fluxes of PVDF and PTFE membranes. Figure 8 showed that if the external mass transfer coefficient including the gas phase and membrane is constant, the increase of liquid velocity brings the increase of CO_2 flux. Also, the CO_2 flux increased with an increase of external mass transfer coefficient, which means a decrease of external resistance at the boundary condition. Figure 9 showed the calculated CO_2 fluxes in the case of

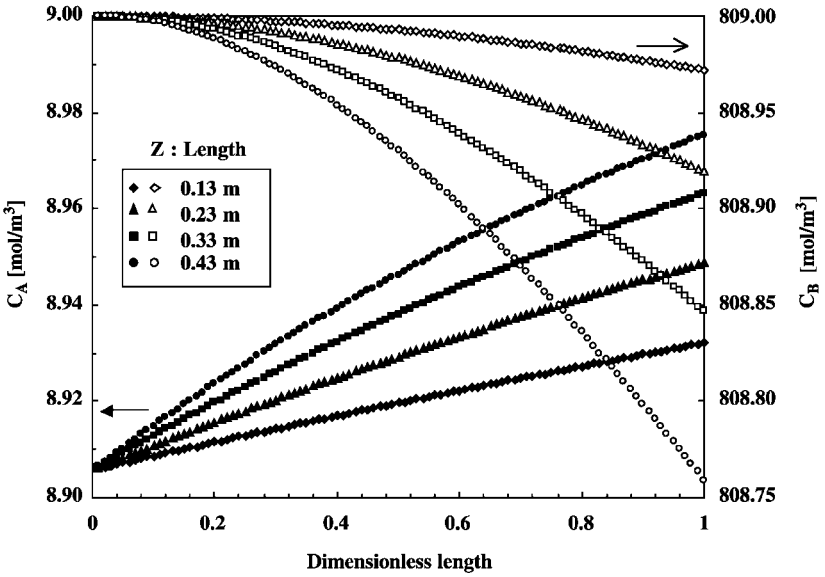

Figure 5. CO_2 and MEA concentration profile as a function of fiber dimensionless length for fibers with different total lengths. Other parameters than fiber length are the same as in Fig. 4.

PTFE membrane. Compared with Fig. 8, at the same external mass transfer coefficient and same velocity, the fluxes in PTFE were lower than those in PVDF. We can predict from these results that the increase of the fiber's diameter causes the decrease of the CO_2 flux because the only different thing about the results is the fiber's diameter.

EXPERIMENTAL

Hybrid Process

The experimental sep-up for CO_2 removal and recovery is shown in Fig. 10, in which it constituted a hybrid process of a membrane contactor and a thermal stripping column. In the case of the absorber, the gas containing 25% of CO_2 (balance N_2) was passed upstream in the tube side of the membrane module and the absorbent of MEA (2-monoethanalamine) 5 wt% was supplied downstream in the shell side. The gas and liquid flow rates were changed at

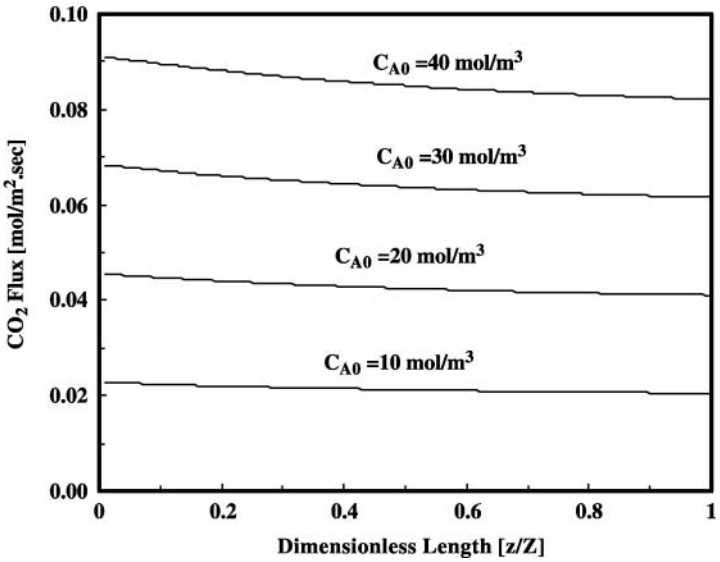

Figure 6. Simulated local flux of CO_2 as a function of fiber dimensionless length for different initial CO_2 concentration in gas phase, C_{AO}. Other parameters than C_{AO} are the same as in Fig. 4.

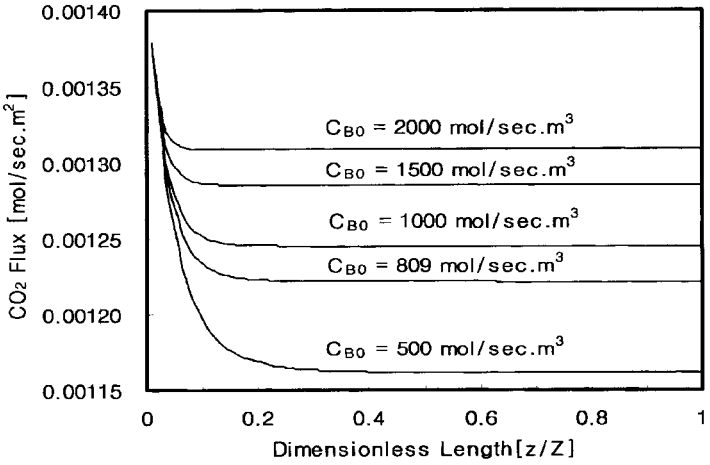

Figure 7. Simulated local flux of CO_2 as a function of fiber dimensionless length for different initial MEA concentrations in liquid phase, C_{BO}. Other parameters than C_{BO} are the same as in Fig. 4.

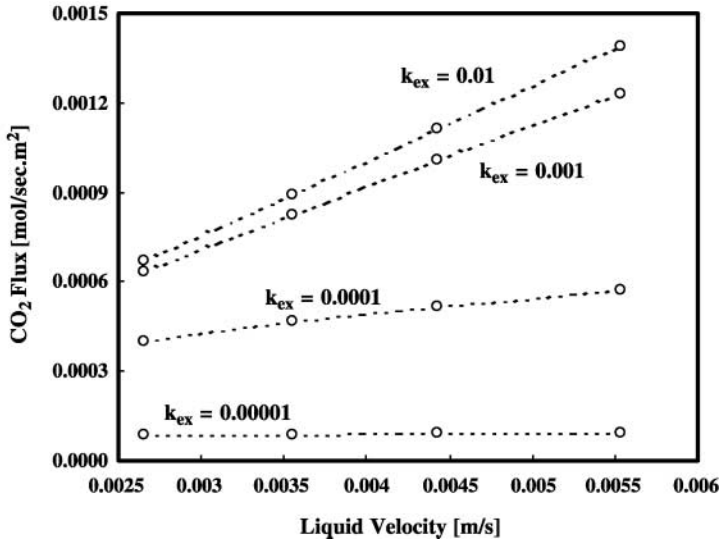

Figure 8. Simulated local fluxes of CO_2 vs. liquid phase velocity in PVDF fiber with different external resistance.

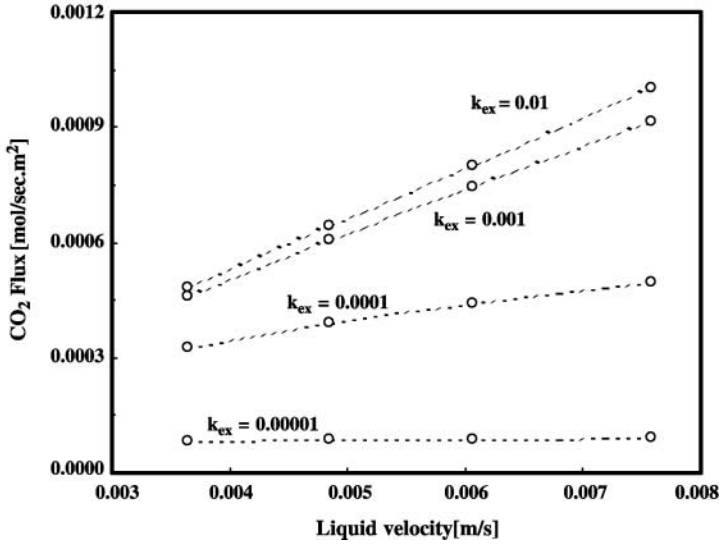

Figure 9. Simulated local fluxes of CO_2 vs. liquid phase velocity in PTFE fiber with different external resistance.

Table 2. Dimension and properties of absorber modules.

	PTFE	PVDF
Module		
Diameter (m)	0.02	0.02
Length (m)	0.23	0.23
Surface area (m^2/m^3)	1339.5	1488.1
Contact area (m^2/m^3)	937.64	—
Volume (cm^3)	72.2	72.2
Fiber		
I.D. (μm)	1000	830
O.D. (μm)	1913	1070
Pore size (μm)	1	0.03
Porosity (%)	70	—
Packing density	0.64	0.4
Number of fibers	70	139

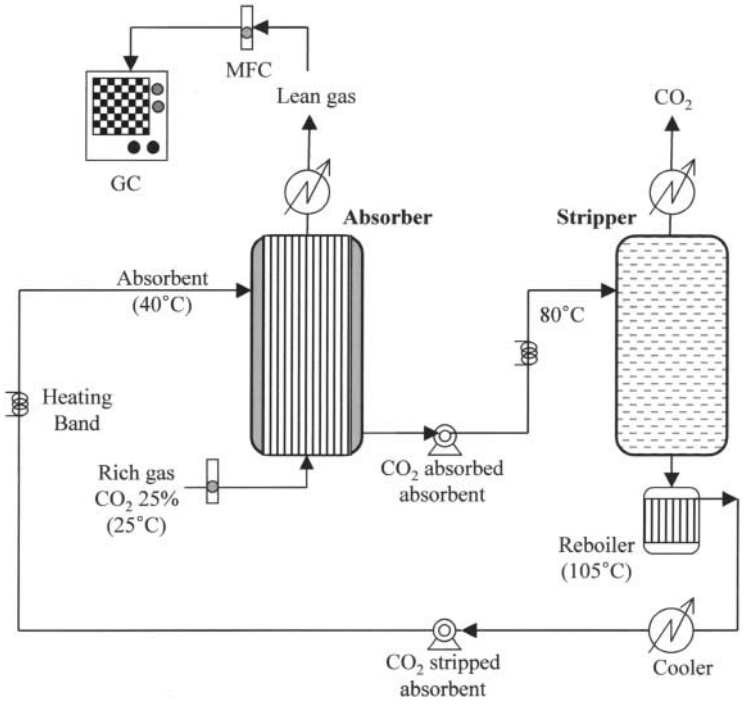

Figure 10. Experimental set up for CO_2 recovery process using absorption.

the range of 100–700 cc/min. and 12–60 cc/min. The MEA solution was reused after the CO_2 dissolved in the solution was totally stripped in the desorption tower connected with the reboiler. The heating band was tied at the inlet of the desorption tower into which the high temperature absorbent flowed to increase the desorption efficiency, and at the top of the tower, the condenser was installed to minimize the evaporation of steam. In the membrane module, the pressure difference of the gas phase and the liquid phase was kept in the range of 2–4 psig by a needle valve to form the stable gas–liquid interface. The gases coming from the absorption and desorption module was analyzed by TCD-GC (GC-14B, Shimadzu).

Absorption and Desorption Module

The membrane contactors used as CO_2 absorbers in this study are the PTFE (polytetrafluoruethylene, Sumitomo Co., Japan) and the PVDF (polyvinylidinefluoride, Krict, Korea) hollow fibers. Table 2 shows the properties for each module. The polymeric hollow fiber materials are basically hydrophobic, but this surface nature may be changed according to the physical properties of the fiber, such as pore size, surface tension, and contact angle against the absorbent used. The porosity of the PTFE fiber that usually has symmetric structure can be calculated through various analyzers, such as SEM and BET, but it is very difficult to measure the porosity of the PVDF fiber due to its asymmetrical structure. Therefore, it is impossible to find out the contact area of the PVDF membrane.

To separate CO_2 dissolved in the absorbent and reuse the absorbent, the desorption module was equipped nearby the absorption module. The desorption tower was made in a sort of glass, and the vacuum surface coated with silver helped prevent heat emission.

EXPERIMENTAL RESULTS

To compare CO_2 removal capacities of PVDF and PTFE membranes, many experiments were conducted under the conditions of different liquid and gas velocities. Figure 11 shows CO_2 removal efficiency and flux of the PVDF membrane. At a constant liquid velocity, the MEA solution can absorb a limited amount of CO_2 no matter by what amount the feed gas is increased. Therefore, the CO_2 removal efficiency decreases with an increase

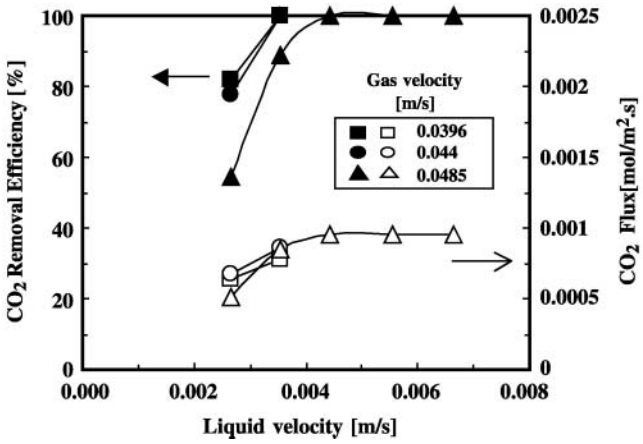

Figure 11. CO_2 removal efficiency and flux of PVDF membrane (MEA 5 wt% solution).

of gas velocity in the range of the efficiency less than 100%. In this range, CO_2 flux is constant regardless of an increase of gas velocity. When the gas velocity is constant, the absorption capacity of the MEA solution is enlarged at a high liquid velocity. Therefore, the removal efficiency of CO_2 increases with an increase of liquid velocity. Finally, it reaches the removal efficiency of 100%. In this range, the CO_2 flux increased initially with an increase of gas velocity. The flux then tended to reach an asymptotic value at high gas velocity.

Figure 12 shows CO_2 removal efficiency and flux in the PTFE membrane module. The CO_2 removal efficiency of the PTFE membrane exhibited the same tendency with Fig. 11, but the CO_2 flux of the PTFE membrane was lower than that of the PVDF membrane at the same gas and liquid velocity. When we compare the CO_2 fluxes of Figs. 11 and 12, the higher flux of the PVDF membrane may result from the interface stability between the gas and liquid phase by the wettibility difference of the absorbent and pores of the fiber surface. Usually, the wettibility of a membrane's pores occurs by the liquid stagnant layer inner the fiber's pores, which depends on the pressure difference of the liquid and gas phase at the membrane's end, namely, critical pressure. This critical pressure which plays an important role in determining the wettibility can be calculated from surface tension, contact angle of membrane's surface, and

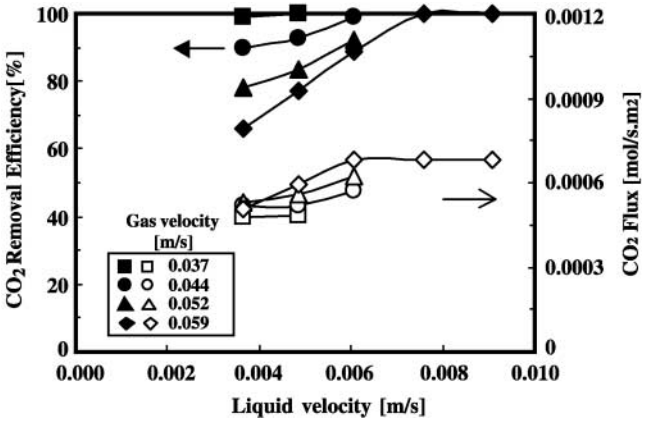

Figure 12. CO_2 removal efficiency and flux of PTFE membrane (MEA 5 wt% solution).

pore size of fiber, as the following Eq. (8).

$$\Delta Pc = -\frac{2(\text{surface tension})(\cos\theta)}{(\text{maximum pore radius})} \tag{8}$$

We can know from Eq. (8) that larger pore size would lower the critical pressure between the gas and liquid phase. In case of the membrane, this low critical pressure means an increase of the wettibility of the membrane pores, which works as a kind of membrane resistance. Therefore, it is expected that the PTFE membrane possessing a relatively large pore size decreases the CO_2 absorption flux by increasing the membrane resistance. It could be proven by observing the phenomena that the absorbent easily penetrates into the gas phase in the absorption test using the PTFE membrane contactor. Hence, we have to control not only the hydrophobic state of membrane, but also the membrane pore size to form the stable interface between the gas and liquid phase

The membrane process has the advantage of a larger surface area than a conventional process, but has a disadvantage such as membrane resistance, in Eq. (2). Therefore, it is important to reduce this resistance in order to improve the removal efficiency of a membrane contactor. Figure 13 shows the comparison of numerical and experimental fluxes in the PVDF and PTFE membranes as a function of liquid velocity. When the numerical external mass transfer coefficients are 0.001 m/s in PVDF and 0.0005 m/s in PTFE, respectively, the results of numerical and experimental fluxes are

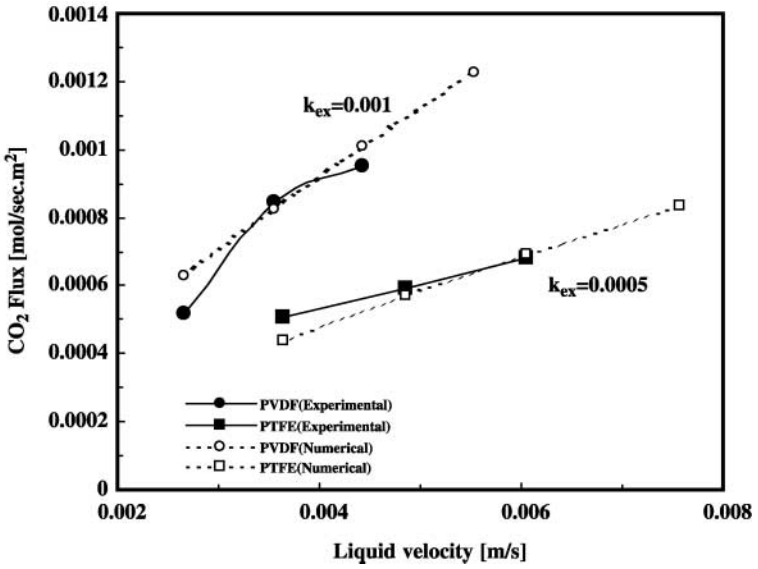

Figure 13. The flux comparison of PTFE and PVDE membranes as a function of liquid velocity.

well agreed. As previously stated, in the numerical result, the PTFE membrane had the lower mass transfer coefficient than the PVDF membrane.

Figure 14 shows the overall mass transfer coefficients that were obtained from Eq. (3) using experimental data. The overall mass transfer coefficient including the fiber's contact area increased with an increase of liquid velocity in both the PVDF and PTFE membrane. Overall mass transfer coefficient, $K_L a$ of a PVDF membrane was three times as much as that of the PTFE. But to compare the real mass transfer capacity of the two membranes, K_L, the contact area is required. As we already mentioned, in Table 2, the contact area of the PVDF membrane could not be calculated due to its asymmetrical structure. Usually, a hollow fiber with an asymmetrical structure shows lower porosity than symmetrical hollow fiber. The effective porosity of the PVDF hollow fiber was studied by Deshmukh[4] who explained that its porosity was less than 48%. Therefore, K_L was obtained by assuming the porosity of the PVDF hollow fiber as 35–40% is shown in Fig. 14. The overall mass transfer coefficient, K_L, in the PVDF membrane showed a higher value than the PTFE membrane.

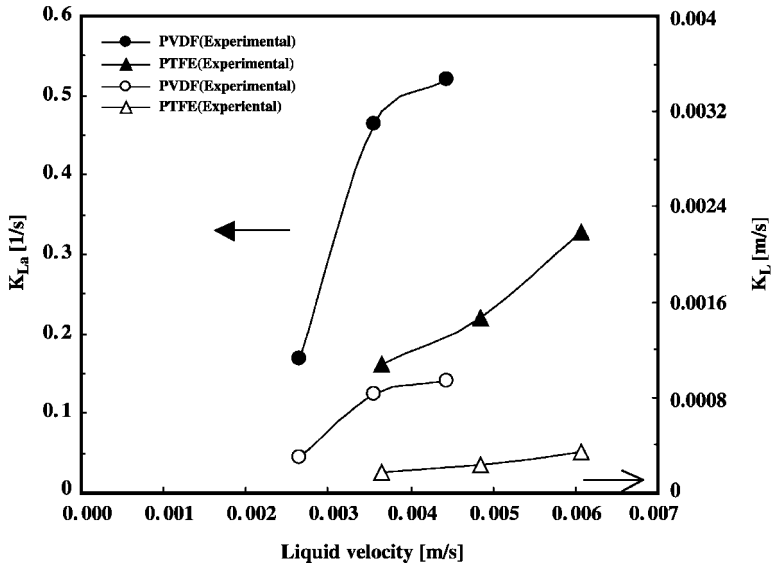

Figure 14. Overall mass transfer coefficient and resistance of liquid phase in PVDF and PTFE membranes as a function of liquid velocity.

We can notice that to gain a high absorption performance in a membrane process, the key factor is not only to enlarge the surface area but also to reduce the total mass transfer resistance for which the membrane resistance accounts for a major portion in some cases.

Figure 15 shows the liquid phase resistance value obtained by increasing the liquid velocity of the PVDF and the PTFE membranes. These values are calculated using Eq. (2b) with the numerical external resistance, k_{ex}, and the experimental overall mass transfer resistance, K_L. When the liquid velocity is about 0.0045 m/s and all the resistances of both PVDF and PTFE hollow fiber membranes are considered, the portions of the external and liquid phase resistance are 18.6% and 1.4%, respectively for the PVDF membrane, and 37.6% and 42.2% for the PTFE membrane, respectively. Since gas phase resistance can be negligible except under the very low gas velocity, the external resistance almost becomes the membrane resistance. Therefore, the membrane mass transfer coefficient in PVDF membrane and in PTFE membrane can be estimated as 0.001 m/s and 0.0005 m/s, respectively.

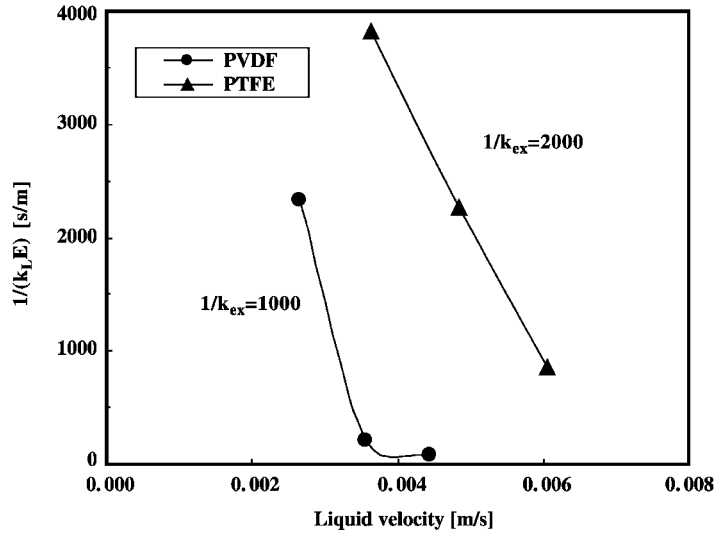

Figure 15. Resistance in the liquid phase as a function of liquid velocity using numerically predicted external resistance.

CONCLUSION

The mass transfer in the carbon dioxide absorption into MEA solution using the PTFE and PVDF hollow fiber membrane contactor was studied numerically and experimentally. The gas absorption system can be simulated with a numerical model assuming an irreversible second order reaction by means of the Crank–Nicholson method. Defining gas phase and membrane resistance as the external resistance, the CO_2 concentration profile in the liquid phase of a fiber was simulated. The mass transfer between the gas and liquid phase is achieved mostly at the wall side of the membrane, in which plenty of small pores are located. The CO_2 flux was simulated in the variation of the initial concentration of the gas–liquid phase, liquid velocity, and external resistance. The CO_2 absorption test using an absorber–stripper hybrid process was conducted and removal efficiency of CO_2 and an overall mass transfer coefficient of the PVDF and PTFE module were determined. The data of the experimental absorption results of carbon dioxide in the MEA absorbent were in agreement with the model predictions and we can predict the external resistance in these membranes. Finally, the liquid phase resistances can be obtained through

the numerical external resistance and experimental overall mass transfer resistance on these two membranes.

NOTATION

Symbols

a	gas–liquid contact area (m^2/m^3)
C_A	concentration of CO_2 in gas phase (mol/m^3)
C_B	concentration of RNH_2 in liquid phase (mol/m^3)
$C_{AO}(C_{Ag})$	initial concentration of component A in gas phase (mol/m^3)
C_{BO}	initial concentration of component B in liquid phase (mol/m^3)
D_A	diffusivity of CO_2 in gas phase (m^2/s)
D_B	diffusivity of RNH_2 in liquid phase (m^2/s)
d_i, d_o	nside and out side diameter of the fiber, respectively (m)
E	enhancement factor (-)
k_1	second-order reaction rate constant (m^3/mol.sec)
K_L	overall liquid phase mass transfer coefficient (m/s)
k_L	liquid phase mass transfer coefficient for chemical absorption (m/s)
k_m	membrane mass transfer coefficient (m/s)
k_g	gas phase mass transfer coefficient (mol/s kPa m^2)
k_{ex}	external mass transfer coefficient (m/s)
P_g, P_i, P_m	CO_2 partial pressures in the bulk gas phase, membrane–liquid interface, and gas–membrane interface, respectively (kPa)
ΔP_{Lm}	log–mean partial pressure driving force (kPa)
m	distribution coefficient (-)
r	radial coordinate (m)
R	fiber radius (m)
v	velocity (m/sec)
y_i, y_o	inlet and outlet CO_2 concentration in the gas phase in mol fraction (-)
Y_{Lm}	log-mean of y_i and y_o in mol fraction (-)
z	axial coordinate (m)
Z	fiber length (m)

Greek Letters

v	stoichiometric coefficient (-)

ACKNOWLEDGMENT

This work was supported by the greenhouse gas research program funding from the Ministry of Science and Technology, Korea.

REFERENCES

1. Desideri, U.; Paolucci, A. Performance modeling of a carbon dioxide removal system for power plants. Energy Convers. Manag. **1999**, *40*, 1899–1915.
2. Rangwala, H.A. Absorption of carbon dioxide into aqueous solutions using hollow fiber membrane contactors. J. Membr. Sci. **1996**, *112*, 229–240.
3. Gabelman, A.; Hwang, S.T. Hollow membrane contactors. J. Membr. Sci. **1999**, *159*, 61–106.
4. Deshmukh, S.P.; Li, K. Effect of ethanol composition in water coagulation bath on morphology of PVDF hollow fiber membranes. J. Membr. Sci. **1998**, *150*, 75–85.
5. Karoor, S.; Sirkar, K.K. Gas absorption studies in microporous hollow fiber membrane modules. Ind. Eng. Chem. Res. **1993**, *32*, 674–684.
6. Kreulen, H.; Smolers, C.; Versteeg, G.F.; van Swaaij, W.P.M. Microporous hollow fiber membrane modules as gas–liquid contactors. Part 1. physical mass transfer processes. J. Membr. Sci. **1993**, *78*, 197–216.
7. Falk-Pesersen, O.; Daninstorm, H. Separation of carbon dioxide from offshore gas turbine exhaust. Energy Convers. Manag. **1997**, *38*, S81–S86.
8. Nii, S.; Takeuchi, H. Removal of CO_2 and/or SO_2 from gas streams by a membrane absorption method. Gas Sep. Purif. **1994**, *8*, 107–114.
9. Nishikawa, N.; Ishibashi, M.; Ohta, H., et al. CO_2 removal by hollow fiber gas–liquid contactor. Energy Convers. Manag. **1995**, *36*, 415–418.
10. Chun, M.S.; Lee, K.-H. Analysis on a hydrophobic hollow fiber membrane absorber and experimental observations of CO_2-removal enhanced absorption. Sep. Sci. Technol. **1997**, *15*, 2445–2466.
11. Yeom, B.Y.; Kim, M.; Lee, Y.; Park, Y.-I.; Lee, K.-H. Absorptioin behavior of carbon dioxide in potassium carbonate aqueous solution

using hollow fiber membrane contactor. HWAHAK KONGHAK (J. Korean Inst. Chem. Eng.) **1998**, *36*, 720–725.
12. Lee, Y.; Park, Y.-I.; Jurn, D.; Lee, Y.; Lee, K.-H. Separation of carbon dioxide by circulatory hollow fiber membrane contactor. HWAHAK KONGHAK (J. Korean Inst. Chem. Eng.) **2000**, *38*, 32–37.
13. Cho, I.-G.; Ahh, H.; Ham, M.; Kim, I.H.; Lee, Y.; Park, Y.-I.; Lee, K.-H. Prediction of absorption behavior of carbon dioxide on membrane contactor. Membr. J. **2000**, *10*, 39–46.
14. Li, K.; Teo, W.K. Use of permeation and absorption methods for CO_2 removal hollow fiber membrane modules. Sep. Purif. Tech. **1998**, *13*, 79–88.
15. Qi, Z.; Cussler, E.L. Microporous hollow fibers for gas absorption, part I,; mass transfer in the liquid. J. Membr. Sci. **1985**, *23*, 321–332.
16. Qi, Z.; Cussler, E.L. Microporous hollow fibers for gas absorption, part II mass transfer across the membrane. J. Membr. Sci. **1985**, *23*, 333–345.
17. Yang, M.C.; Cussler, E.L. Designing hollow fiber contactors. AIChE J. **1986**, *32*, 1910–1915.
18. Bhaumik, D.; Majumdar, S.; Sirkar, K.K. Absorption of CO_2 in a transverse flow hollow fiber membrane module having a few wraps of the fiber mat. J. Membr. Sci. **1998**, *138*, 77–82.
19. Lee, Y.; Noble, R.D.; Yeom, B.-Y.; Park, Y.-I.; Lee, K.-H. Analysis of CO_2 removal by hollow fiber membrane contactors. J. Membr. Sci. **2001**, *194*, 57–67.
20. Kreulen, H.; Smolders, C.A.; Versteeg, G.F.; Van Swaaj, W.P.M. Microporous hollow fiber membrane modules as gas–liquid contactors. Part 2. mass transfer with chemical reaction. J. Membr. Sci. **1993**, *78*, 217–238.
21. Mason, E.A.; Malinauskas, A.P. *Gas transport in porous media: the dusty gas model*, Chem. Eng. Monograph 17; Elsevier: Amsterdam, NL, 1983.
22. Kreulen, H.; Smoldwes, C.A.; Versteeg, G.E.; Van Swaaij, W.P.M. Determination of mass transfer rates in wetted and non-wetted microporous membranes. Chem. Eng. Sci. **1993**, *48*, 2093–2101.
23. Hikita, H.; Ishikawa, H.; Uku, K.; Murakami, T. Diffiusivity of mono-, di-, and triethanolamines in aqueous solution. J. Chem. Eng. Data **1980**, *25*, 324–325.
24. Laddha, S.S.; Danckwerts, P.V. Reaction of CO_2 with ethanolamines; kinetics from gas-absorption. Chem. Eng. Sci. **1981**, *36*, 479–482.

25. Tsai, T.-C.; Ko, J.-J.; Wang, H.-M.; Lin, C.-Y.; Li, M.-H. Solubility of nitrous oxide in alkanolamine aqueous solution. J. Chem. Eng. Data **2000**, *45*, 341–347.
26. Kim, Y.-S.; Yang, S.-M. Absorption of carbon dioxide through hollow fiber membranes using various aqueous absorbents. Sep. Purif. Tech. **2000**, *21*, 101–109.
27. Versteeg, G.F.; van Swaaij, W.P.M. Solubility and diffusivity of acid gases (CO_2, N_2O) in aqueous alkanolamines solutions. J. Chem. Eng. Data **1988**, *33*, 29–34.
28. Gabelman, A.; Hwang, S.-T. Hollow fiber membrane contactors. J. Membr. Sci. **1999**, *159*, 61–106.

Received January 2002
Revised May 2002